

© The Author(s), 2021. Published by Cambridge University Press for the Arizona Board of Regents on behalf of the University of Arizona. This is an Open Access article, distributed under the terms of the Creative Commons Attribution licence (<http://creativecommons.org/licenses/by/4.0/>), which permits unrestricted re-use, distribution, and reproduction in any medium, provided the original work is properly cited.

TIME-INTEGRATED COLLECTION OF CO₂ FOR ¹⁴C ANALYSIS FROM SOILS

Shawn Pedron^{1*}  • X Xu¹  • J C Walker² • J C Ferguson³ • R G Jespersen⁴ • J M Welker^{4,6,7} • E S Klein⁵ • C I Czimczik^{1*} 

¹Department of Earth System Science, University of California, Irvine, CA, USA

²A. E. Lalonde AMS Laboratory, Ottawa, ON, Canada

³Environment and Natural Resources Institute, University of Alaska, Anchorage, USA

⁴Department of Biological Sciences University of Alaska, Anchorage, USA

⁵Department of Geological Sciences University of Alaska, Anchorage, USA

⁶University of Oulu, Oulu, Finland

⁷UArctic, Rovaniemi, Lapland, Finland

ABSTRACT. We developed a passive sampler for time-integrated collection and radiocarbon (¹⁴C) analysis of soil respiration, a major flux in the global C cycle. It consists of a permanent access well that controls the CO₂ uptake rate and an exchangeable molecular sieve CO₂ trap. We tested how access well dimensions and environmental conditions affect collected CO₂, and optimized cleaning procedures to minimize ¹⁴CO₂ memory. We also deployed two generations of the sampler in Arctic tundra for up to two years, collecting CO₂ over periods of 3 days–2 months, while monitoring soil temperature, volumetric water content, and CO₂ concentration. The sampler collects CO₂ at a rate proportional to the length of a silicone tubing inlet (7–26 μg CO₂-C day⁻¹-m Si⁻¹). With constant sampler dimensions in the field, CO₂ recovery is best explained by soil temperature. We retrieved 0.1–5.3 mg C from the 1st and 0.6–13 mg C from the 2nd generation samplers, equivalent to uptake rates of 2–215 (*n*=17) and 10–247 μg CO₂-C day⁻¹ (*n*=20), respectively. The method blank is 8 ± 6 μg C (mean ± sd, *n*=8), with a radiocarbon content (fraction modern) ranging from 0.5875–0.6013 (*n*=2). The sampler enables more continuous investigations of soil C emission sources and is suitable for Arctic environments.

KEYWORDS: carbon, mineral soil, molecular sieve, soil respiration.

INTRODUCTION

Soil respiration, the emission of carbon dioxide CO₂ from soils, is a major flux in the global carbon (C) cycle, and its radiocarbon content (here reported as fraction modern carbon (*F*) (Trumbore et al. 2016)) allows insights to the cycling of C in terrestrial ecosystems (Trumbore 2009). The *F* of soil respiration (soil *FCO*₂) is a measure of the amount of time that has passed since the constituent C atoms were last in the atmosphere, integrating the transit through various reservoirs, including plant and microbial biomass, soil organic matter, and carbonates (Sierra et al. 2017).

In organic and acidic soils, soil *FCO*₂ provides an important constraint on how rapidly soils may sequester or lose organic C in response to changes in net primary productivity or environmental conditions (Shi et al. 2020). Along with its δ¹³C signature (Hicks Pries et al. 2013), soil *FCO*₂ can be used to partition soil C emissions into contributions from the rhizosphere (respiration of roots and associated microorganisms) relative to those from microorganisms that decompose soil organic matter to reveal how plant and microbial activity and microbial C sources are influenced by changes in environmental conditions (Trumbore 2006, 2000; Hicks Pries et al. 2013).

Many investigations of soil *FCO*₂ collect net soil respiration from chambers or soil pore space CO₂ from gas wells (Borker et al. 2006; Czimczik et al. 2006; Schuur and Trumbore 2006;

*Corresponding authors. Emails: czimczik@uci.edu; spedron@uci.edu

Estop-Aragónés et al. 2018; Hicks Pries et al. 2017, 2013; Lupascu et al. 2014a). However, these methods use pumps or evacuated canisters and accumulate CO₂ prior to collection, which can affect the gradient of CO₂ within the soil profile and may change soil FCO₂. These approaches also collect CO₂ about once a month over periods of minutes to about one day and may miss episodic C emissions (Muhr et al. 2010; Lupascu et al. 2014b). Furthermore, most soil respiration source studies in seasonal environments have focused on the growing season. The scarcity of time-integrated and non-growing season data is of particular concern in high latitude ecosystems (Lupascu et al. 2018; Natali et al. 2019), where permafrost soils with vast C stocks are rapidly warming and active layer depths are changing (Box et al. 2019; Pulliainen et al. 2020). Thus, the evaluation of environmental change on C cycling in soils over time and across landscapes could be improved by more continuous and passive measurements of soil FCO₂.

To achieve time-integrated samples, gas intake rates into evacuated steel canisters have traditionally been modulated by adjusting the length and inner diameter of a critical flow path, i.e. a capillary (Lupascu et al. 2014c; Trumbore et al. 2015; Walker et al. 2015). In cold environments, however, a capillary upstream from the membrane is likely to become obstructed by condensing or freezing water vapor. Our sampler uses a tubular diffusive membrane intake to exclude liquid water while transmitting gas. Passive CO₂ trapping for ¹⁴CO₂ analysis is a technique with increasing use and popularity (Walker et al. 2015; Wotte et al. 2017a, 2017b). Trace-gas sampling wells and chambers with passive CO₂ traps have been used with diffusive silicone (Si) membranes in periodically saturated soils and waters since 2001 (Jacinthe and Groffman 2001; Kammann et al. 2001; Garnett et al. 2009; Wotte et al. 2017a), and modified to perform depth-resolved C isotope sampling in peatlands (Clymo and Bryant 2008; Garnett et al. 2012, 2011) and mineral soils (Hartley et al. 2013). Here, we adapted such a sampler for usage in upland environments (mineral soil) without soil collars (trenching). Our sampler is designed to be permanently installed year-round in extreme conditions (−36 to +15°C, ice-bound to 100% volumetric water content (VWC)), with negligible routine maintenance and easy and efficient exchange of CO₂ traps to capture winter and shoulder-season (spring/autumn) permafrost dynamics. Fully steel components (excluding PTFE ferrules for airtight connections and Si tubing) and cold- and vacuum-rated valves ensure high durability and accuracy in the harsh winter. We also investigate some environmental predictors (VWC, temperature, CO₂ concentration CO₂) that likely relate to sampling rate and soil respiration *F* and δ¹³C values.

We present a rugged and lightweight sampler that collects soil CO₂ passively (capturing CO₂ by diffusion) for subsequent *F* (and δ¹³C) analysis over periods of two weeks to two months from soil depths of 20–80 cm below the surface. We designed the sampler to withstand Arctic conditions, including freeze-thaw cycles, waterlogging, and herbivory, in a remote location without power. Our method allows the collection of soil FCO₂ year-round to provide seasonal to annual estimates of C cycling rates in terrestrial ecosystems.

METHODS

CO₂ Isotope Sampler

The sampler consists of a soil gas access well (“access well”) that is permanently installed in the soil, and an exchangeable, rechargeable molecular sieve trap (“MS trap”) to capture soil CO₂ for C isotope (*F* and δ¹³C) analysis (Figure 1). The soil gas inlet (Figure 1A) is composed of a platinum-cured Si rubber tube (1 m, ¼” OD, 2124T5, McMaster-Carr, USA), which forms a membrane between the interior of the tubing and the (semi-) saturated soil surrounding it.

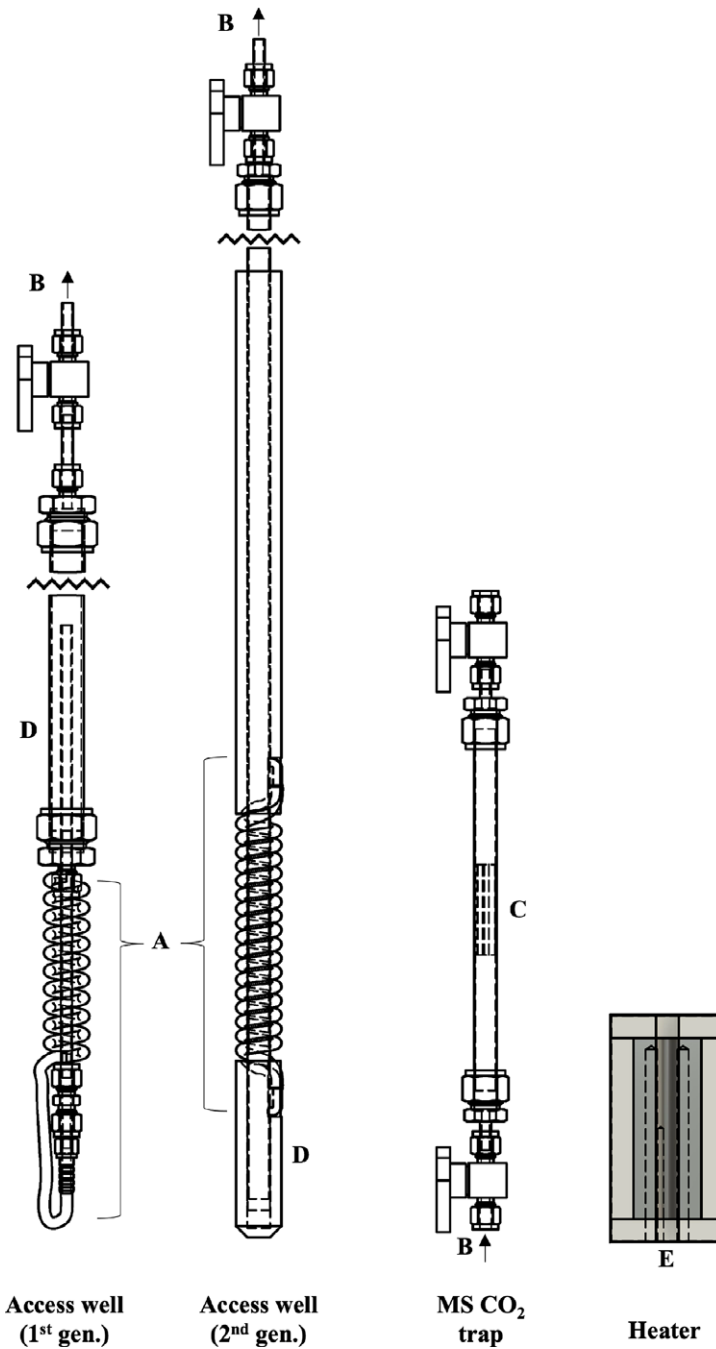


Figure 1 Soil ¹⁴CO₂ sampler components consisting of a permanently installed access well (2 generations), exchangeable MS trap, and CO₂ extraction heater. Soil CO₂ passes through gas-permeable silicone tubing (A) and passively diffuses along flow path through junction (B) to be adsorbed upon molecular sieve (C). Interior ice deposits melt and pool in sump (D) in spring. CO₂ is thermally desorbed in laboratory using clamshell-style heaters (E).

Silicone rubber (and other Si-polymeric membranes) are known to be permeable to many gases, with gas-specific permeability proportional to molecular diameter and temperature (Kammermeyer 1957; Robb 1968). The tubing excludes liquid water but allows gas to diffuse into the sampler without disturbing the CO₂ gradient within the soil profile. Diffusivity of CO₂ in Si rubber is governed by Fick's law, whereby diffusion of a gas across a fluid barrier (the Si tube) is a function of the concentration difference across the barrier, the barrier thickness, and the (temperature-dependent) diffusion coefficient of the gas (Bertoni et al. 2004). The length of the tubing which we use directly translates to a greater surface area over which diffusion can occur. Diffusivity is also determined by the polarity of the material and permeating gas molecule (Zhang and Cloud 2006), which should make (polar, hydrophobic) Si effective at reducing water vapor uptake.

Two generations of inlets were used. In the original version, Si tubing is sealed on one end and connected to the sampler via a ¼" hose connection. This connects to ¼" OD stainless steel tubing that passes through a bore-through connection to the interior of a ¾" OD tube to create a water sump (Figure 1D), which prevents the obstruction of the gas flow path by ice or water from water vapor permeating the inlet and condensing or freezing along the inner walls.

In the optimized 2nd version, Si tubing is coiled around the sampler and connected at both ends by a steel 90° elbow tube silver-soldered to the interior of a 1.5 m long ½" OD smooth-bore stainless-steel tube. This central steel tubing ends above ground and is capped 5 cm below the Si coil to create the water sump (Figure 1D). After soldering on the bottom cap, the steel tubing is washed with 20% HCl (#7647-01-0, Klean Strip Green, USA) and rinsed with MQ water. The steel tubing sections above and below the Si coil, which are expected to be below the soil surface, are sleeved with PVC tubing (1" OD, ½" ID) to seal the hole augured into the soil for well insertion to minimize gas flux in the vertical axis. All wells in the 2nd gen. are the same length to maintain a consistent internal diffusion path, independent of how deep they are inserted in the soil.

A junction (Figure 1B) spanning two plug valves (PTFE components and Si-based lubricant, SS-4P4T, Swagelok, USA) connects the access well to a removable MS trap and enables MS trap exchanges without exposure of the interior of the access well to ambient atmosphere. Expected snow depths determine the overall length of the access wells. Prior to attaching the first MS trap, each access well is evacuated to -25" Hg pressure with a hand pump (MITMV8500, MightyVac, USA).

The design and extraction technique of the MS trap was based on work by Walker et al. (2015). With open valves, CO₂ is collected by sorption onto pre-cleaned zeolite MS (Figure 1C; 1.5 g, 45–60 mesh, 13X, 20304 Sigma-Aldrich, USA) contained within a 316 stainless steel mesh envelope (0.114 mm ID mesh opening, 9419T34, McMaster-Carr, USA). The envelope is folded to contain the zeolite and stay in place through friction with the interior of a steel tube (½" OD, 8" length) that is pre-baked at 550°C in air for 1 hr (to oxidize any residual organics from fabrication) and capped with ½" to ¼" reducers and SS-4P4T valves. All connections are stainless steel to avoid differential expansion. Alternatively, soil gas can be collected from the access well with an evacuated steel canister.

Laboratory Analyses of CO₂

We built two clamshell-style heaters to thermally desorb CO₂ from MS traps in the laboratory (Figure 1E). One half of each heater was built by installing insertion heaters (4877133 x2,

McMaster-Carr, USA) and a high-temperature thermocouple (9353k31, McMaster-Carr, USA) into an insulated steel block. Two symmetrical halves were both connected to a digital temperature control (sensitivity $\pm 2^\circ\text{C}$, SL4848-RR, AutomationDirect, USA) to form a full heater. The MS trap is clamped within a heater and attached to a vacuum line, where CO₂ is extracted under vacuum at 425°C for 30 min, cryogenically purified, and graphitized using a sealed-tube zinc reduction method (Xu et al. 2007). The extraction is followed by a cleaning sequence at 500°C with 100 mL min⁻¹ UHP N₂ flush for 20 min, then 100 mL min⁻¹ UHP CO₂-free (zero) air flush for 10 min. After cleaning, the MS trap is pressurized to just over 1 atm with UHP zero air to minimize leaking caused by pressure changes during air transport.

For samples with a total yield >0.3 mg C, an aliquot of CO₂ is split and analyzed for ¹³C (GasBench II coupled with DeltaPlus XL, Thermo, USA). The ¹⁴C of the graphite is measured with accelerator mass spectrometry (NEC 0.5MV 1.5SDH-2 AMS) alongside processing standards and blanks at the KCCAMS laboratory of UC Irvine (Santos et al. 2007; Beverly et al. 2010).

We report stable isotope measurements using conventional δ notation (‰) (Equation 1):

$$\delta^{13}\text{C} = 1000 \cdot \left(\frac{R_{\text{sample}}}{R_{\text{standard}}} - 1 \right) \quad (1)$$

Where R_{sample} denotes the heavy-to-light isotope ratio of a sample and R_{standard} is the isotope ratio of the standard (0.0112372 for Vienna Pee Dee Belemite (PDB) ¹³C/¹²C standard (Gonfiantini 1984). We report radiocarbon results using the fraction modern (F) notation (Equation 2):

$$F = \frac{R_{\text{SN}}}{R_{\text{ON}}} = \frac{R_{\text{S}} \left(\frac{0.975}{1 + \delta/1000} \right)^2}{0.95R_{\text{O,-19}}} \quad (2)$$

Where R_{SN} is the measured ¹⁴C/¹²C ratio of the sample normalized for fractionation to a $\delta^{13}\text{C}$ value of -25‰ , with δ being the measured $\delta^{13}\text{C}$ value of the sample, and R_{ON} is the ¹⁴C/¹²C ratio of the oxalic acid I standard measured in 1950 ($1.176 \pm 0.010 \cdot 10^{-12}$), normalized for fractionation to its measured $\delta^{13}\text{C}$ value of -19‰ (Trumbore et al. 2016). The measurement uncertainty for all samples and standards was $<0.003 F$ based on long-term reproducibility of secondary standards.

Sampler Performance

We took three approaches to evaluate the samplers: (1) We examined isotope sampling accuracy and potential memory effect on both the standalone MS traps and full-process replications by collecting pure certified reference material standards for up to 24 hr and periods of 1–4 weeks, respectively. (2) We optimized access well dimensions for sample intake rate by attaching varied lengths of Si membrane and Bev-A-Line (56280, 1/8" ID x 1/4" OD Bev-A-Line IV, United States Plastic Corp., USA) to evacuated steel canisters and MS traps. To further test sampling rate and gas seal, we exposed the full-process replications to varied CO₂ and temperature. (3) We evaluated real-world performance by deploying a complete sampler in the field for two years.

Table 1 Summary statistics for standard material tests on MS traps. *Known* values are accepted literature consensus *F* values, and measured $\delta^{13}\text{C}$ of pure aliquots (‰); 2-tailed Student's t-test p-values use the *Known* value as true.

	Standard	MS trap					
		Known	Mean	st.dev	st.err	N	p-value
OX II	<i>F</i>	1.341	1.328	0.005	0.002	4	0.011
	$\delta^{13}\text{C}$	-17.4	-17.3	0.1	0.1	4	0.652
OX I	<i>F</i>	1.040	1.038	0.004	0.001	24	0.013
	$\delta^{13}\text{C}$	-19.0	-18.8	0.2	0.0	16	0.000
TIRI-B	<i>F</i>	0.571	0.570	0.002	0.001	4	0.349
	$\delta^{13}\text{C}$	-24.5	-24.4	0.1	0.1	4	0.277
Coal	<i>F</i>	0.000	0.003			1	
	$\delta^{13}\text{C}$	-23.1	-22.9			1	

(1) *Isotope sampling.* To assess the suitability of each MS trap for isotope analysis, we compared the C isotope data of reference materials analyzed with and without MS trap exposure. As “known” values, we used literature consensus *F* values, and measured $\delta^{13}\text{C}$ of pure aliquots (Table 1). Specifically, we used two modern oxalic acid standard materials OX I (SRM4990B) and OX II (SRM4990C) (Mann 1983), one aged wood standard, (TIRI B) (Scott 2003), and one ^{14}C -free material (ABA-cleaned bituminous coal, USGS Pocahontas #3) (Trent et al. 1982; Xu et al. 2007). These reference materials were combusted to CO_2 , purified, and allowed to passively transfer onto each MS trap on a vacuum line. After 12–24 hr, CO_2 was extracted and measured for *F* and $\delta^{13}\text{C}$ (see section Laboratory Analysis of CO_2). To quantify potential memory effects (i.e., “hysteresis,” CO_2 that survives the post-extraction cleaning), some traps were tested multiple times, so that standards with known signatures (0.571–1.040 *F*, $n = 12$; -23.1 to -19.4‰ $\delta^{13}\text{C}$, $n = 5$) could be compared to values of the previous samples held by those traps.

A MS trap method blank was evaluated from a set of MS traps that were subjected to the entire sampling process aside from actual exposure to soil CO_2 , in order to capture the average contaminating CO_2 intrusion which may leak into a MS trap in routine sampling. MS traps were shipped to the field site filled with ~ 1 atm UHP CO_2 -free air, attached to access wells (but never opened), and shipped back to the lab (58–59 days, $n = 8$). These were extracted and used to calculate the size and *F* of the method blank (only 2 were large enough for ^{14}C , but not ^{13}C analysis).

Full-process replications were created by enclosing Si inlet assemblies (as in Figure 1A, 1st gen.) in sealed glass mason jars with ports through which the internal atmosphere could be evacuated and then filled with CO_2 . These full-process sampler + jar systems were evacuated to $<10^{-2}$ torr and filled with 1 atm UHP zero air, and reference material was injected into the jars and allowed to diffuse into the samplers for 1–4-weeks ($n = 20$). We evaluated the response of the measured isotopes to varied ambient CO_2 (0.33–0.71%), temperature (-20 and 20°C), path length (0.03–1.3 m), and unique reference material signature (0.571–1.040 *F*; -24.5 to -19.04‰ $\delta^{13}\text{C}$) by varying the amount of reference material injected into each jar, and either enclosing the mason jar in a freezer or leaving it at lab temperature. We used stepwise optimization of multivariate linear regression models (*R* *step* and *lm* functions, *stats* v3.6.2 package) to determine the unbiased significance of

each predictor variable to each response (F , $\delta^{13}\text{C}$, sampling rate). By using Akaike information criteria to eliminate irrelevant predictors, we arrived at multivariate models for each response that maximized goodness of fit while minimizing model complexity.

(2) *Access well.* We optimized several access-well components in the laboratory to maximize the CO₂ uptake rate in intermittently waterlogged and frozen soil without disturbing the CO₂ gradient. First, we tested the influence of Si surface area, diffusion path length, and collection system (canister or MS trap) by attaching diffusive Si tubing (0–3 m, sealed on one end) to gas-impermeable Bev-A-Line tubing (0–3 m). This well-prototype was connected to MS traps and, or 0.5, 6, or 32 L evacuated stainless-steel canisters and exposed to ambient CO₂ ($n=41$). The uptake rate was calculated by extracting CO₂ after 1–58 days. We selected Si tubing lengths up to the maximum amount that could be installed without causing dramatic site disturbance, and path lengths that would allow us to access the collection system above typical snowpack heights.

Second, we evaluated the predictive value of CO₂, temperature, and path length on the sampling rate response for the same full-process replications described in *Isotope sampling*.

(3) *Field sampling.* To assess the performance of the sampler in the field, we continuously collected soil CO₂ from a moist acidic tussock (dominated by *Eriophorum vaginatum* L./wet sedge (*Carex bigelowii*) tundra (O horizon pH = 3.7 ± 0.1 , B horizon 4.6 ± 0.4 mean \pm se (Hobbie and Gough 2002)) near Toolik Field Station, AK, USA (68.625478 N, 149.602199 W, 724 m, -6.8 to -5.8°C MAT, 44 to 52 cm yr⁻¹ MAP 2017–2019) between June 2017 and August 2019. The values presented here are from samplers that were part of a larger experiment, but we focus only on assessing the sampler performance.

The 1st gen. access well ($n = 1$) was installed at 20 cm below the surface in June 2017. Soil gas samples were collected over 3–6 weeks in evacuated canisters (0.5–32 L) from June 2017 to September 2017, with MS traps from September 2017 to 2018, and with alternating MS traps and evacuated canisters from September 2018 to August 2019. Episodically ($n = 6$), when $F\text{CO}_2$ was also measured using traditional sampling approaches with dynamic chambers ($n = 42$) as described in Lupascu et al. (2014a), we also collected gas samples over 3–6 days in 0.5 L evacuated canisters. The 2nd gen. access wells ($n = 20$) were installed between 20 and 80 cm depth in July 2019 and were only sampled over 8 weeks with MS traps.

To gauge the sampler's efficiency and quantify the temporal variability of soil pore space CO₂, we co-deployed CO₂ (non-dispersive infrared, Carbocap GMP343 with vertical soil attachment and PTFE membrane, Vaisala, Finland) and VWC and temperature probes (VWC from dielectric permittivity, temperature from thermistor, Decagon 5TM, METER, USA) with the 1st gen. access well ($n = 1$ each at -20 cm). CO₂ data were collected from June 2017 to August 2019 at 30-s resolution on a computer, using software made in LabVIEW (Laboratory Virtual Instrument Engineering Workbench, National Instruments, USA, 2017) to simply capture data output from the probes and save it to a text file located on a cloud drive. A CO₂ temperature-correction was applied by the GMP343 firmware at the time of measurement. VWC and temperature data were collected from September 2017 to August 2019 at 15-min resolution and stored on a Decagon Em50 battery-powered data logger and accessed during field campaigns.

We evaluated the response of the measured isotopes and sample collection rate to the dynamic soil environment. We again used stepwise optimization of a multivariate linear regression

model to determine the significance of each predictor variable. These include the mean of measured environmental predictors over each sampling period (CO_2 , VWC, temperature), state of water at the depth of the gas inlet, and the collection system used. Sample collection rate was also considered as a predictor for ^{13}C and ^{14}C . Where gaps in the data existed due to sensor malfunction or differences in installation date, the day-of-year means over the sampling period ($\sim 2\%$ of CO_2 , $\sim 7\%$ of VWC and temperature data) were used.

Data Corrections

We corrected the measured C isotopes for three likely sources of exogenous C: method blank (full-process replications and field samples), contaminating lab-air CO_2 dissolved in Si tubing (full-process replications only), and mixing of ambient air CO_2 into soil (field samples only). Calculated method blank or air fractions (i.e., impurities) were used to correct isotope values (Equation 3):

$$\Delta_{\text{sample}} = \Delta_{\text{impurity}} \cdot f_{\text{impurity}} + \Delta_{\text{corrected}} \cdot (1 - f_{\text{impurity}}) \quad (3)$$

Where Δ represents either $F\text{CO}_2$ or $\delta^{13}\text{CO}_2$. Calculated fractions were also used to correct yield (and thereby sampling rate) (Equation 4):

$$\text{Yield}_{\text{corrected}} = \text{Yield}_{\text{sample}} - \text{Yield}_{\text{sample}} \cdot f_{\text{impurity}} \quad (4)$$

We corrected samples with yields < 1 mg C for method blanks using the blank size and F (see *Isotope sampling*). Given a fixed blank value, the significance of the blank to the total sample signature will decrease as the sample size increases. With our blank F (0.5875, 0.6013, $n = 2$) and size (8.5 ± 6 $\mu\text{g C}$, $n = 8$), blank corrections for samples > 1 mg C would approach our analytical uncertainty (0.003 F). MS trap results were not corrected for $\delta^{13}\text{C}$ method blanks.

To account for lab-air CO_2 that was dissolved in the Si tubing used for full-process replications, we calculated the total mass of CO_2 which was dissolved in the Si tubing at the experimental start time given the tubing dimensions and an approximate solubility of $2.2 \text{ m}^3 \text{ CO}_2 \text{ m}^{-3} \text{ Si atm}$ (Robb 1968). We then took the ratio of this mass to the total yield for the contaminating fraction ($< 7\%$ for all samples). We assume that the isotopic composition of the lab air was similar to that of the field air given that: CO_2 is a well-mixed gas, lab-air measured no more than 600 ppm when testing the GMP343 probes, and human-respired $\delta^{13}\text{CO}_2$ is not different enough from ambient (approximately -22% vs. -9% respectively; Affek and Eiler 2006) to have a large effect on the correction.

To account for mixing of ambient air CO_2 into soil, which dilutes the soil respiration isotope signatures, we calculated the fraction of air present in the soil over each sampling period as the ratio between CO_2 in ambient air (from Imnavait, about 8 km away) and at the inlet depth. The isotopic composition of the field air was measured at the site during campaigns ($n = 11 F\text{CO}_2$, $n = 10 \delta^{13}\text{CO}_2$) as described in Lupascu et al. (2014a).

RESULTS AND DISCUSSION

(1) *Isotope sampling*. Our MS traps allowed for reproducible and accurate C isotope measurements of CO_2 . The mean standard error for three reference materials (OXI, OXII, and TIRI-B) absorbed upon standalone MS traps was 0.0014 F and 0.056‰ $\delta^{13}\text{C}$ (Figure 2A, B, Table 1). F of the recovered reference materials was not very different from

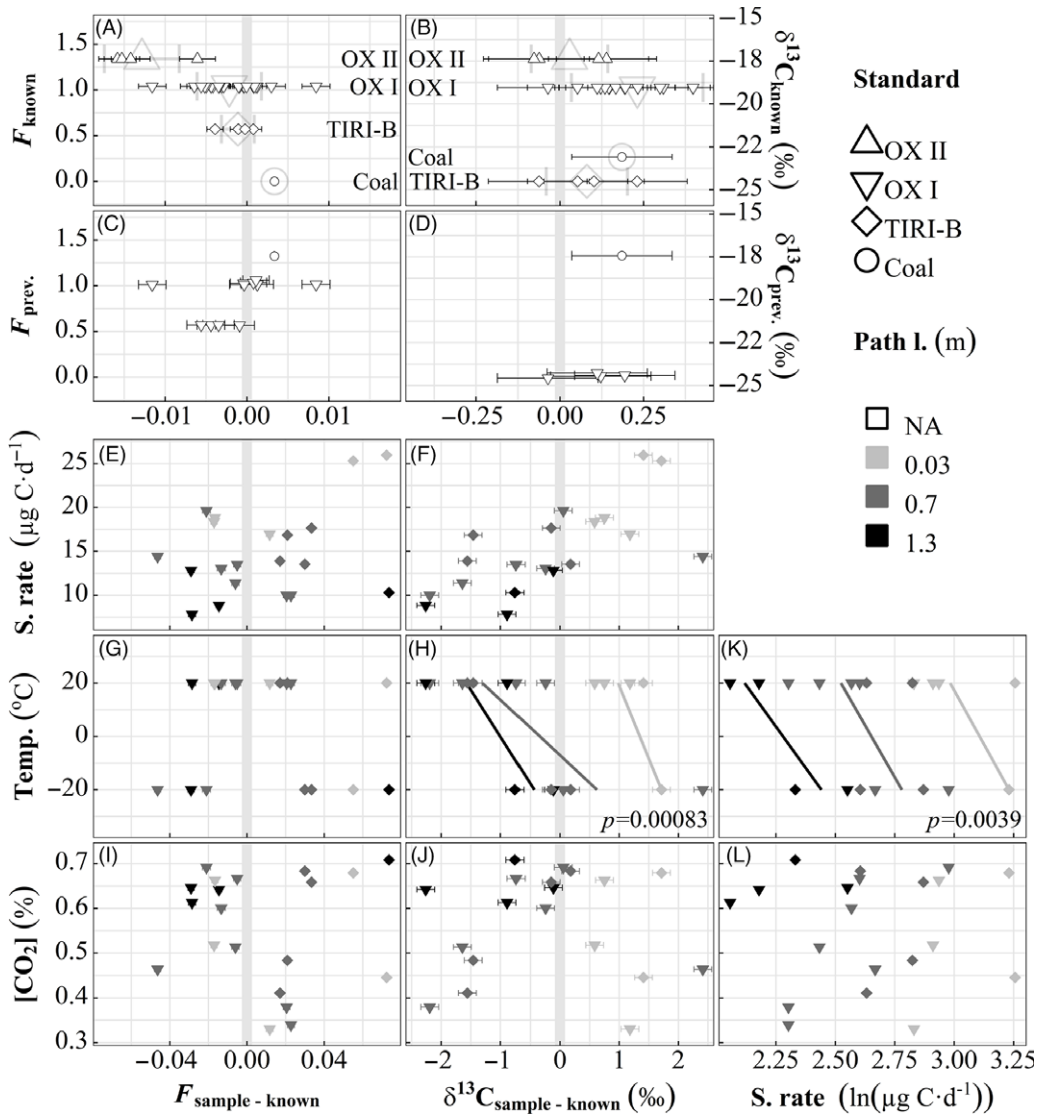


Figure 2 Recovery of reference materials from standalone and full-process tests of CO₂ traps. A–J: Deviation of recovered isotope values from known values of F_{CO_2} and $\delta^{13}C_{CO_2}$ of reference materials (grey vertical band shows no difference). Small error bars show instrumental error (1σ). A–D: Open symbols, performance of standalone MS traps (0.18–0.92 mg C). A, B show recovery of pure reference material for standalone traps (on top of large light-grey standard mean \pm sd), and C, D show this relative to a trap's previous sample value. E–L: Closed symbols, performance of full-process replications as a function of relevant predictors. Regressions and significance level are shown for significant predictors as determined by stepwise minimization of Akaike information criterion. For full-process replicates, reference material signature is significant for F deviation, and path length and temperature are significant for $\delta^{13}C$ deviation and sampling rate (all $p < 0.004$).

their consensus values (Table 1). Although the two-tailed Student's t -test indicated a p -value only slightly greater than 0.01 for two of the standards, the greatest mean difference (i.e., sample-known values, $0.013 \pm 0.002 F$ for OXII) is less than the standard deviation of full-process replicates ($0.020 F$ for OXI, $0.024 F$ for TIRI-B, Figure 2E, G, I), indicating

that ^{14}C error of MS traps is less than that of individual samples. Only one bituminous coal standard was run as an extreme test of sorption hysteresis; it is shown in Figure 2A–D. $\delta^{13}\text{C}$ was greater than pure aliquot values by $<0.5\%$ consistently. It is known that MS material fractionates $\delta^{13}\text{C}$ upon absorption (Davidson 1995; Garnett and Hardie 2009), with a typical value of 4% under ambient CO_2 . It is likely that we do not see this magnitude of fractionation because pure CO_2 was used, and therefore absorption was not inhibited or slowed by non-absorbable gases (N_2 and O_2) as it would be in atmospheric or soil gas environments. Additionally, the diffusion pathway between the vacuum extraction line and the MS traps was short, and complete absorption only took <5 min. Wotte et al. (2017b) also report insignificant $\delta^{13}\text{C}$ fractionation for their testing of a similar MS trap design. We observe no hysteresis for ^{14}C or ^{13}C (Figure 2C, D), which would be evident as a strong linear relationship between previous signature and current deviation from known. The MS trap blank (not shown) was $8 \pm 6 \mu\text{g C}$, equivalent to $0.15 \pm 0.11 \mu\text{g C day}^{-1}$ (mean \pm sd, $n = 8$), with F of 0.5875 and 0.6013 ($n = 2$).

The deviation from known is larger for full-process replications (Figure 2E–J) than for standalone MS traps. It is likely that our attempt to create a controlled ambient environment around the inlets resulted in an imperfect seal, causing recovered reference materials to deviate towards the value of ambient air (Northern Hemisphere $F\text{CO}_2$ was 0.98 in 2013 (Reimer et al. 2013), while atmospheric $\delta^{13}\text{CO}_2$ is approximately -9%). This is most apparent in F results: TIRI-B samples were more enriched than known, while OX I were more depleted (known F of 0.571 and 1.040, respectively). The larger deviation of samples taken at -20°C leads us to believe that the suboptimal seal on the mason jar intended to contain the ambient atmosphere was exacerbated by different thermal expansion coefficients of the jar materials (i.e., metal will contract more than glass). Stepwise regression assigns significance to the reference material signature for ^{14}C , and temperature and path length for ^{13}C . We see no influence of sampling rate, temperature, or CO_2 on F , and no radical values that would reveal methodological contamination. The significant temperature + path length $\delta^{13}\text{C}$ trend (Figure 2H) is likely the combined result of air leakage from imperfect seal and fractionation along the diffusive path from inlet to MS material, as it is not evident in (fractionation-corrected) F results (Figure 2G). This observed fractionation may contribute to the $\sim 4\%$ $\delta^{13}\text{C}$ depletion reported in previous research on passive MS trapping (Davidson 1995; Garnett and Hardie 2009). While it appears to be correctable, we will not attempt to do so until the phenomenon is better understood.

(2) *Access well.* In the prototyping tests, the CO_2 sampling rate varied from 7–44 $\mu\text{g C day}^{-1}$ depending on Si tubing length and path length, temperature, CO_2 , and to a smaller degree, on collector (canister or MS trap). We found sampling rate to be directly related to Si tubing length and inversely to path length (Figure 3A). At equivalent Si and path lengths and temperatures, the rate for canisters (which actively draw all ambient gas into the sampler with negative pressure) is 3.7 ± 1 (mean \pm sd, $n = 17$) times greater than for MS traps, which adsorb CO_2 molecules passively diffusing into the sampler. We also observe a small direct sampling rate proportionality to canister volume (not shown), however it was far outweighed by the other controls.

A Si tubing length of 1 m was chosen to optimize sampling rate while minimizing site disturbance, producing reasonable yields over a range of path lengths for sampling periods >2 weeks given the anticipated soil CO_2 . Stepwise regression assigns significance to

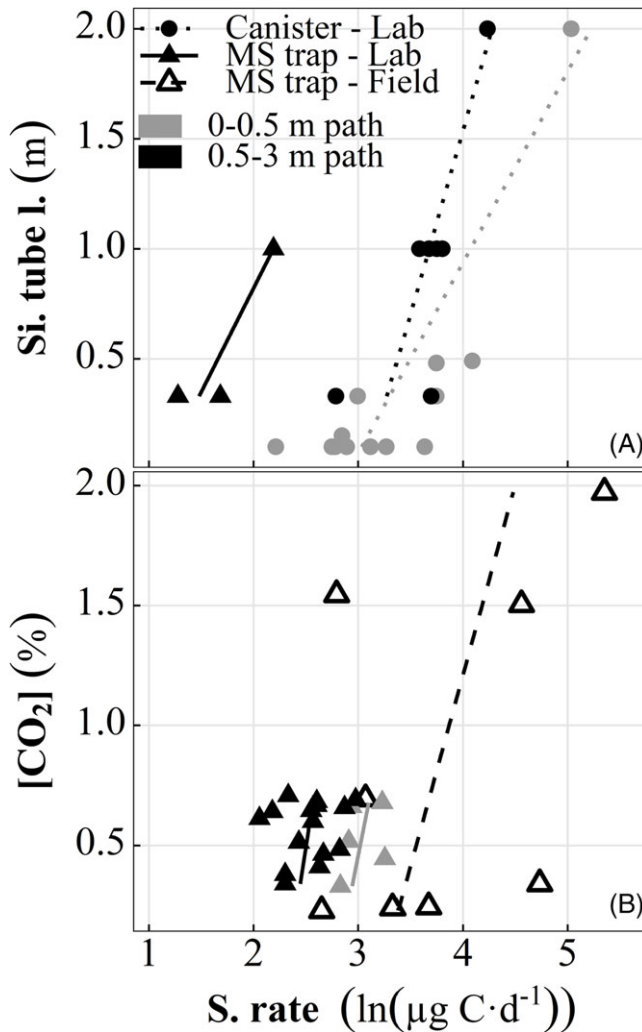


Figure 3 Response of CO₂ sampling rate to (A) varied silicone inlet lengths at equivalent CO₂ (lab only) and (B) varied ambient CO₂ at equivalent silicone tubing length of 1 m (lab and field at temperatures >0°C). Path length is from inlet connection to MS trap joint.

temperature and path length as predictors of sampling rate (Figure 2K). We transform (natural log) sampling rate here and throughout the figures for easy comparison with field results, which demonstrate bimodal distribution (i.e., frozen vs. thawed) and a strong exponential relationship between sampling rate and temperature (Figure 4E). The inverse temperature effect on sampling rate was unexpected, as CO₂ permeability of Si rubber *increases* with increasing temperature (a dramatic reduction is only seen below approximately -40°C; Robb 1968). The most likely explanation is once more the poor seal of the mason jars containing the inlets, allowing more freezer air to enter the system. This potentially contributes to the temperature dependence of ¹³C as well. If the influence of temperature on sampling rate is ignored, CO₂ becomes a significant predictor in a simple linear model of CO₂ and path length ($p = 0.03$, Figure 3B, solid symbols).

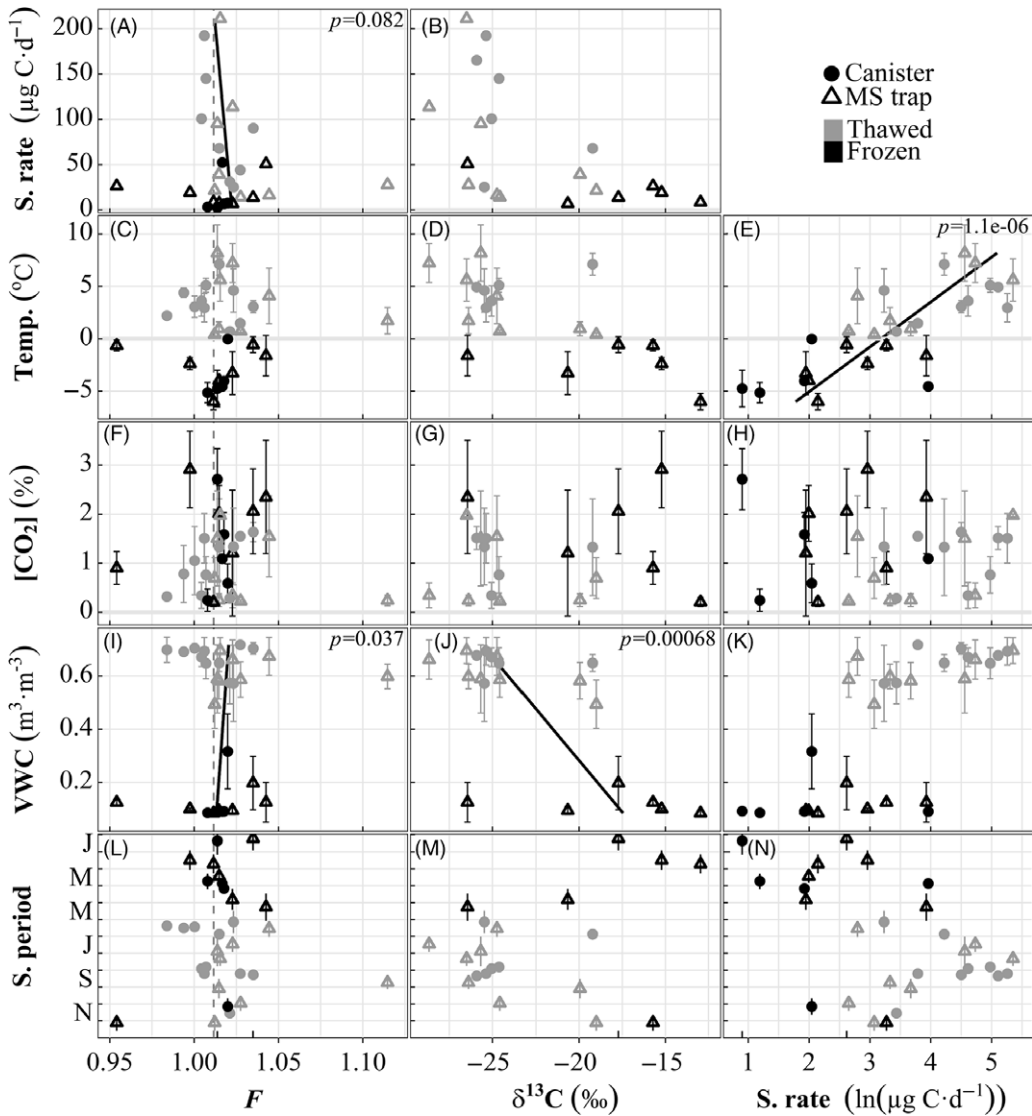


Figure 4 Response of 2 years of soil CO₂ *F*, δ¹³C, and sampling rate (one sampler, depth = -20 cm) to relevant predictors. Bars for *Sampling period* panels (L–N) span on and off dates. Error bars of environmental predictor panels (C–K) show standard deviation of the predictor over the sampling period. Regressions are shown for predictors that maximize the quality of a multivariate linear regression for each response (x-axes). The vertical dashed line for *F* is the mean value for ambient air over the experimental period (6 ± 8%, *n* = 9).

(3) *Field sampling.* In the field, at temperatures >0°C, the response of the sampler’s CO₂ uptake rate to varying CO₂ (i.e. slope) was comparable to that in the lab (Figure 3B, open symbols). We observed more variable CO₂ uptake rates (7.0–45 μg C day⁻¹ lab vs. 2.5–210 μg C day⁻¹ field) in the field, likely due to a much broader CO₂ range (0.33–0.71% lab vs. 0.063–4.7% field) and changes in environmental conditions such as soil VWC (9.2–79%), temperature (–8.1–13°C), and pore space volume with freeze-thaw cycles. While our calibrations focused on the most significant controls of sampling rate, future

investigations should also consider soils with different textures to understand the influence of soil moisture and pore space volume. The approximate maximum adsorption capacity for 13X zeolite MS (25°C at 100 kPa, without water vapor) is ~4 mol CO₂ kg⁻¹ zeolite based on experimental data on adsorption equilibria (Wang and LeVan 2009), which equates to a maximum of 72 mg CO₂-C given the 1.5 g of zeolite material used in our MS traps. The range of uncorrected yields captured on MS traps attached to 1st gen. access wells in this experiment was 0.087–5.3 mg CO₂-C, and 0.56–13 mg CO₂-C on 2nd gen. access wells using the same MS traps. The higher 2nd-gen. yields are likely due to more methodical coiling of Si tubing and the dual ports to the interior diffusion pathway, as well as greater sampling periods. Since all samples collected over the two-year period were less than half the capacity of the MS trap, we assume that sample uptake was linear over each sampling period.

Our three models of field-collected FCO_2 , $\delta^{13}CO_2$, and sampling rate considered CO₂, VWC, temperature, water state of matter, and collector type as predictor variables (Figure 4). The CO₂, state of water, and collector used did not significantly influence any response. Sample collection rate was calculated as the total yield over the collection period, and was strongly responsive to temperature (Figure 4E). When samples collected at subzero temperatures are considered (as opposed to Figure 3B field samples), CO₂ loses significance as a predictor of sampling rate, but still appears to have bimodal linear responses for frozen and thawed states, implying unique summer and winter controls on sampling rate (Figure 4H). We theorize that winter reductions in sampling rate are due to reduced microbial and plant respiration, followed by restriction of soil C transport when soil water freezes (Mikan et al. 2006; Lee et al. 2010). It is known that the availability of liquid water in soils near freezing temperatures is a strong control on microbial activity (Schimel and Clein 1995). Like Lee et al. (2010), we observe extremely high CO₂ in the months before the start of the growing season—likely due to a reduction of the pore volume near the CO₂-sensor—without a corresponding spike in sampling rate. The CO₂ permeability of Si rubber is a direct function of temperature, in the same direction as the observed trend. However, the magnitude is much smaller than what we observe. According to (Robb 1968), Si rubber has permeabilities of 323 and 293 cc cm s⁻¹ cm² cm Hg at temperatures of 28 and -40°C, respectively. This equates to a linear slope of 0.14% permeability per °C, while our observed range of CO₂ sampling rate spans 3 orders of magnitude.

Although we do not see the same sampling-rate-dependent $\delta^{13}C$ fractionation in the field that was evident in full-process replications, further work is needed to explore this effect. The VWC dependence of $\delta^{13}CO_2$ (Figure 4J) could be related to physical or microbial processes. For example, kinetic fractionation occurs in the partitioning between gas-phase and dissolved CO₂ (Thode et al. 1965), resulting in enrichment in the gas phase, which is inversely proportional to temperature. It is also known that microbial methanogenesis processes yield CO₂ enriched in $\delta^{13}C$ (Whiticar et al. 1986; Aravena et al. 1993; Charman et al. 1999), which is also an inverse function of temperature. While we have observed local indicators of methanogenesis (blue-grey mineral soil, bubbles in nearby standing water), and the environment is likely suitable (anoxia caused by frequent inundation and/or continuous winter snowpack), we did not directly collect any methane.

Soil FCO_2 is not strongly correlated to any predictor variables (all $p > 0.03$), but does show some seasonality and the model is improved when predicted by VWC and sampling rate (Figure 4L, I, and A respectively). The sampling rate correlation is logical, as maximum

sampling rates are observed during the peak growing season (Figure 4N), when autotrophic respiration (modern F) is greatest. $F\text{CO}_2$ of field samples during the growing season (1.021 ± 0.031 mean \pm sd, $n = 15$, June–September) varied similarly to the observed $F\text{CO}_2$ of traditional soil respiration chambers ($1.040 \pm 0.026\%$ mean \pm sd, $n = 39$) measured during campaigns. The sampler signature at 20 cm depth is near enough to the soil surface to be close to representative of the growing season isotopic flux but is also able to capture older C (oldest sample $F = 0.954\%$, November/December 2018) during the non-growing season. As plant respiration slows at the end of the growing season and soil water freezes to ice, heterotrophs become confined to their local environment. This corresponds with a change in available substrate from more modern, labile C (i.e. plant exudates and litter from the growing season) (Grogan and Chapin 1999) to older C which is potentially still easily degradable and high in carbohydrates (Mueller et al. 2015), due to a history of physical vertical mixing from freeze-thaw cycles common to tundra ecosystems (Schimel and Clein 1995; Bockheim 2007). Winter and shoulder-season (i.e. spring and autumn) fluxes of ancient C have also been seen in high-latitude forests (Winston et al. 1997; Hirsch et al. 2002; Czimczik et al. 2006), peatlands (Garnett and Hardie 2009), and tundra (Hartley et al. 2013; Hicks Pries et al. 2013; Lupascu et al. 2018b). Our sampler offers a device capable of capturing a continuous year-round record of soil CO_2 isotopes in permafrost environments.

CONCLUSIONS

We present a novel sampler designed for time-integrated, year-round collection of soil-respired CO_2 and subsequent C isotope analysis in remote environments that facilitates a deeper understanding of C cycling in soils, i.e., plant and microbial contributions to soil-atmosphere CO_2 fluxes and microbial C sources. Soil CO_2 diffuses into the sampler via a water-proof Si membrane and accumulates in lightweight, compact MS traps, but can also be collected in evacuated canisters. The CO_2 collection rate is proportional to soil temperature. The deployment of the sampler in Arctic tundra demonstrates its ruggedness and suitability for use in organic and mineral soils and sediments with a wide range of moisture and temperature conditions.

ACKNOWLEDGMENTS

We thank the Toolik Field Station Science Support and Environmental Data Center teams, D. Helmig (CU Boulder), and the KCCAMS staff and C. McCormick (UCI) for their logistical and technical support. Funding was provided by the U.S. NSF OPP (#1649664 to C.I.C., #1650084 to J.M.W. and E.S.K.).

REFERENCES

- Affek HP, Eiler JM. 2006. Abundance of mass 47 CO_2 in urban air car exhaust and human breath. *Geochimica et Cosmochimica Acta* 70(1) 1–12.
- Aravena R, Warner BG, Charman DJ, Belyea LR, Mathur SP, Dinel H. 1993. Carbon isotopic composition of deep carbon gases in an ombrogenous peatland northwestern Ontario, Canada. *Radiocarbon* 35(2):271–276.
- Bertoni G, Ciuchini C, Tappa R. 2004. Measurement of long-term average carbon dioxide concentrations using passive diffusion sampling. *Atmospheric Environment* 38(11):1625–1630.
- Beverly RK, Beaumont W, Tauz D, Ormsby KM, von Reden KF, Santos GM, Southon JR, Reden KF, Von Santos GM, Southon JR. 2010. The Keck Carbon Cycle AMS laboratory, University of California Irvine: status report. *Radiocarbon* 52(2):301–309.
- Bockheim JG. 2007. Importance of cryoturbation in redistributing organic carbon in permafrost-affected

- soils. *Soil Science Society of America Journal* 71(4): 1335–1342.
- Borker W, Savage K, Davidson E, Trumbore SE. 2006. Effects of experimental drought on soil respiration and radiocarbon efflux from a temperate forest soil. *Global Change Biology* 12: 177–193.
- Box JE, Colgan WT, Schmidt NM, Lund M, Parmentier F-JW, Brown R, Bhatt US, Euskirchen ES, Romanovsky VE, Walsh JE, et al. 2019. Key indicators of Arctic climate change: 1971–2017. *Environmental Research Letters* 14(4):045010.
- Charman DJ, Aravena R, Bryant CL, Harkness DD. 1999. Carbon isotopes in peat DOC CO₂ and CH₄ in a Holocene peatland on Dartmoor southwest England. *Geology* 27(6):539–542.
- Clymo RS, Bryant CL. 2008. Diffusion and mass flow of dissolved carbon dioxide methane and dissolved organic carbon in a 7-m deep raised peat bog. *Geochimica et Cosmochimica Acta* 72(8):2048–2066.
- Czimczik CI, Trumbore SE, Carbone MS, Winston GC. 2006. Changing sources of soil respiration with time since fire in a boreal forest. *Global Change Biology* 12(6):957–971.
- Davidson GR. 1995. The stable isotopic composition and measurement of carbon in soil CO₂. *Geochimica et Cosmochimica Acta* 59(12): 2485–2489.
- Estop-Aragonés C, Czimczik CI, Heffernan L, Gibson C, Walker JC, Xu X, Olefeldt D. 2018. Respiration of aged soil carbon during fall in permafrost peatlands enhanced by active layer deepening following wildfire but limited following thermokarst. *Environmental Research Letters* 13:085002.
- Garnett MH, Dinsmore KJ, Billett MF. 2012. Annual variability in the radiocarbon age and source of dissolved CO₂ in a peatland stream. *Science of the Total Environment* 427–428 (May):277–285.
- Garnett MH, Hardie SML. 2009. Isotope (¹⁴C and ¹³C) analysis of deep peat CO₂ using a passive sampling technique. *Soil Biology and Biochemistry* 41(12):2477–2483.
- Garnett MH, Hardie SML, Murray C. 2011. Radiocarbon and stable carbon analysis of dissolved methane and carbon dioxide from the profile of a raised peat bog. *Radiocarbon* 53:71–83.
- Garnett MH, Hartley IP, Hopkins DW, Sommerkorn M, Wookey PA. 2009. A passive sampling method for radiocarbon analysis of soil respiration using molecular sieve. *Soil Biology and Biochemistry* 41(7):1450–1456.
- Gonfiantini R. 1984. Stable isotope reference samples for geochemical and hydrological investigations. *The International Journal of Applied Radiation and Isotopes* 35(5):426.
- Grogan P, Chapin FS. 1999. Arctic soil respiration: Effects of climate and vegetation depend on season. *Ecosystems* 2(5):451–459.
- Hartley IP, Garnett MH, Sommerkorn M, Hopkins DW, Wookey PA. 2013. The age of CO₂ released from soils in contrasting ecosystems during the arctic winter. *Soil Biology and Biochemistry* 63:1–4.
- Hicks Pries CE, Castanha C, Porras RC, Torn MS. 2017. The whole-soil carbon flux in response to warming. *Science* 355(6332):1420–1423.
- Hicks Pries CE, Schuur EAG, Crummer KG. 2013. Thawing permafrost increases old soil and autotrophic respiration in tundra: Partitioning ecosystem respiration using δ¹³C and Δ¹⁴C. *Global Change Biology* 19(2):649–661.
- Hirsch AI, Trumbore SE, Goulden ML. 2002. Direct measurement of the deep soil respiration accompanying seasonal thawing of a boreal forest soil. *Journal of Geophysical Research: Atmospheres* 107(D3):8221–8231.
- Hobbie SE, Gough L. 2002. Foliar and soil nutrients in tundra on glacial landscapes of contrasting ages in northern Alaska. *Oecologia* 131(3):453–462.
- Jacinte PA, Groffman PM. 2001. Silicone rubber sampler to measure dissolved gases in saturated soils and waters. *Soil Biology and Biochemistry* 33(7–8):907–912.
- Kammann C, Grünhage L, Jäger H-J. 2001. A new sampling technique to monitor concentrations of CH₄, N₂O and CO₂ in air at well-defined depths in soils with varied water potential. *European Journal of Soil Science* 52(2):297–303.
- Kammermeyer K. 1957. Silicone rubber as a selective barrier. *Industrial and Engineering Chemistry* 49(10):1685–1686.
- Lee H, Schuur EAG, Vogel JG. 2010. Soil CO₂ production in upland tundra where permafrost is thawing. *Journal of Geophysical Research* 115(G1).
- Lupascu M, Czimczik CI, Welker MC, Ziolkowski LA, Cooper EJ, Welker JM. 2018. Winter ecosystem respiration and sources of CO₂ from the High Arctic tundra of Svalbard: Response to a deeper snow experiment. *Journal of Geophysical Research: Biogeosciences* 123(8): 2627–2642.
- Lupascu M, Welker JM, Seibt U, Maseyk K, Xu X, Czimczik CI. 2014a. High Arctic wetting reduces permafrost carbon feedbacks to climate warming. *Nature Climate Change* 4(1):51–55.
- Lupascu M, Welker JM, Seibt U, Xu X, Velicogna I, Lindsey DS, Czimczik CI. 2014b. The amount and timing of precipitation control the magnitude seasonality and sources (¹⁴C) of ecosystem respiration in a polar semi-desert northwestern Greenland. *Biogeosciences* 11(16): 4289–4304.
- Lupascu M, Welker JM, Xu X, Czimczik CI. 2014c. Rates and radiocarbon content of summer ecosystem respiration in response to long-term deeper snow in the High Arctic of NW Greenland. *Journal of Geophysical Research: Biogeosciences* 119(6):1180–1194.

- Mann WB. 1983. An international reference material for radiocarbon dating. *Radiocarbon* 25(2): 519–527.
- Mikan C, Schimel JP, Michaelson G, Welker J, Romanovsky VE, Fahnestock J, Ping C-L. 2006. Cold-season production of CO₂ in Arctic soils: Can laboratory and field estimates be reconciled through a simple modeling approach? *Arctic Antarctic and Alpine Research* 38(2): 249–256.
- Mueller CW, Rethemeyer J, Kao-Kniffin J, Löppmann S, Hinkel KM, Bockheim J. 2015. Large amounts of labile organic carbon in permafrost soils of northern Alaska. *Global Change Biology* 21(7):2804–2817.
- Muhr J, Franke J, Borken W. 2010. Drying-rewetting events reduce C and N losses from a Norway spruce forest floor. *Soil Biology and Biochemistry* 42(8):1303–1312.
- Natali SM, Watts JD, Rogers BM, Potter S, Ludwig SM, Selbmann AK, Sullivan PF, Zona D, et al. 2019. Large loss of CO₂ in winter observed across the northern permafrost region. *Nature Climate Change* 9(11):852–857.
- Pulliainen J, Luojus K, Derksen C, Mudryk L, Lemmetyinen J, Salminen M, Ikonen J, Takala M, Cohen J, Smolander T, Norberg J. 2020. Patterns and trends of Northern Hemisphere snow mass from 1980 to 2018. *Nature* 581(7808): 294–298.
- Reimer PJ, Bard E, Bayliss A, Beck JW, Blackwell PG, Bronk Ramsey C, Buck C, Cheng H, Edwards RL, Friedrich M, Grootes PM, Guilderson TP, Hafliðason H, Hajdas I, Hatté C, Heaton TJ, Hoffmann DL, Hogg AG, Hughen KA, Kaiser KF, Kromer B, Manning SW, Niu M, Reimer RW, Richards DA, Scott EM, Southon JR, Staff RA, Turney CSM, van der Plicht J. 2013. IntCal13 and Marine13 radiocarbon age calibration curves 0–50,000 years cal BP. *Radiocarbon* 55(4): 1869–1887.
- Robb WL. 1968. Thin silicone membranes—their permeation properties and some applications. *Annals of the New York Academy of Sciences* 146(1):119–137.
- Santos GM, Southon JR, Griffin S, Beaupre SR, Druffel ERM. 2007. Ultra small-mass AMS ¹⁴C sample preparation and analyses at KCCAMS/UCI Facility. *Nuclear Instruments and Methods in Physics Research Section B: Beam Interactions with Materials and Atoms* 259(1): 293–302.
- Schimel JP, Clein JS. 1995. Microbial response to freeze-thaw cycles in tundra and taiga soils. *Soil Biology and Biochemistry* 28(8):1061–1066.
- Schuur EAG, Trumbore SE. 2006. Partitioning sources of soil respiration in boreal black spruce forest using radiocarbon. *Global Change Biology* 12(2):165–176.
- Scott EM. 2003. Part 2: the Third International Radiocarbon Intercomparison (TIRI). *Radiocarbon* 45(2):293–328.
- Shi Z, Allison SD, He Y, Levine PA, Hoyt AM, Beem-Miller J, Zhu Q, Wieder WR, Trumbore S, Randerson JT. 2020. The age distribution of global soil carbon inferred from radiocarbon measurements. *Nature Geoscience* 13(8):555–559.
- Sierra CA, Müller M, Metzler H, Manzoni S, Trumbore SE. 2017. The muddle of ages turnover transit and residence times in the carbon cycle. *Global Change Biology* 23(5):1763–1773.
- Thode HG, Shima M, Rees CE, Krishnamurthy KV. 1965. Carbon-13 isotope effects in systems containing carbon dioxide bicarbonate carbonate and metal ions.
- Trent VA, Medlin JH, Coleman SL, Stanton RW. 1982. Chemical analyses and physical properties of 12 coal samples from the Pocahontas field Tazewell County Virginia and McDowell County West Virginia. U.S. Geological Survey Bulletin 1528.
- Trumbore S, Czimczik CI, Sierra CA, Muhr J, Xu X. 2015. Non-structural carbon dynamics and allocation relate to growth rate and leaf habit in California oaks. *Tree Physiology* 35(11): 1206–1222.
- Trumbore SE. 2000. Age of soil organic matter and soil respiration: Radiocarbon constraints on belowground C dynamics. *Ecological Applications* 10(2):399–411.
- Trumbore SE. 2006. Carbon respired by terrestrial ecosystems - recent progress and challenges. *Global Change Biology* 12(2):141–153.
- Trumbore SE. 2009. Radiocarbon and soil carbon dynamics. *Annual Review of Earth and Planetary Sciences* 37(1):47–66.
- Trumbore SE, Sierra CA, Hicks Pries CE. 2016. Radiocarbon nomenclature theory models and interpretation: Measuring age determining cycling rates and tracing source pools. In: *Radiocarbon and climate change: mechanisms applications and laboratory techniques*. Springer International Publishing. p. 45–82.
- Walker JC, Xu X, Fahrni SM, Lupascu M, Czimczik CI. 2015. Developing a passive trap for diffusive atmospheric ¹⁴CO₂ sampling. *Nuclear Instruments and Methods in Physics Research Section B: Beam Interactions with Materials and Atoms* 361:632–637.
- Wang Y, LeVan MD. 2009. Adsorption equilibrium of carbon dioxide and water vapor on zeolites 5a and 13X and silica gel: pure components. *Journal of Chemical and Engineering Data* 54(10):2839–2844.
- Whiticar MJ, Faber E, Schoell M. 1986. Biogenic methane formation in marine and freshwater environments: CO₂ reduction vs. acetate fermentation-Isotope evidence. *Geochimica et Cosmochimica Acta* 50(5):693–709.

- Winston GC, Sundquist ET, Stephens BB, Trumbore SE. 1997. Winter CO₂ fluxes in a boreal forest. *Journal of Geophysical Research Atmospheres* 102(24):28795–28804.
- Wotte A, Wischhöfer P, Wacker L, Rethemeyer J. 2017a. ¹⁴CO₂ analysis of soil gas: evaluation of sample size limits and sampling devices. *Nuclear Instruments and Methods in Physics Research Section B: Beam Interactions with Materials and Atoms* 413:51–56.
- Wotte A, Wordell-Dietrich P, Wacker L, Don A, Rethemeyer J. 2017b. ¹⁴CO₂ processing using an improved and robust molecular sieve cartridge. *Nuclear Instruments and Methods in Physics Research Section B: Beam Interactions with Materials and Atoms* 400:65–73.
- Xu X, Trumbore SE, Zheng S, Southon JR, McDuffee KE, Luttgen M, Liu JC. 2007. Modifying a sealed tube zinc reduction method for preparation of AMS graphite targets: reducing background and attaining high precision. *Nuclear Instruments and Methods in Physics Research Section B: Beam Interactions with Materials and Atoms* 259(1): 320–329.
- Zhang H, Cloud A. 2006. In SAMPE Fall Technical Conference: Global Advances in Materials and Process Engineering Coating and Sealants Section. p. 1–10.